Nanoscale Structuring of Semiconducting Molecular Blend Films in the Presence of Mobile Counterions

Jakob Heier,*[,†] Jan Groenewold,*[,‡] Simon Huber,[†] Frank Nüesch,[†] and Roland Hany[†]

Laboratory for Functional Polymers, Swiss Federal Laboratories for Materials Testing and Research (EMPA), Überlandstrasse 129, 8600 Dübendorf, Switzerland, and Physical & Colloid Chemistry, University of Utrecht, Padualaan 8, 3584CH Utrecht, The Netherlands

Received January 11, 2008. Revised Manuscript Received March 14, 2008

The controlled fabrication of submicrometer phase-separated morphologies of semiconducting organic materials is attracting considerable interest, for example, in emerging thin-film optoelectronic device applications. For thin films of spin-coated blends of PCBM ([6,6]-phenyl-C_{61}-butyric acid methyl ester) and cationic cyanine dyes, we used atomic force microscopy scans to infer the structure formation mechanism: The solutions separate into transient bilayers, which further spinodally destabilize because of long-range molecular interactions. A thin layer ruptures earlier than a thick layer, and the earlier instability determines the morphology. Consequently, the resulting morphology type mainly depends on the ratio of the layer thicknesses, whereas the periodicity of structures is determined by the absolute film thickness. These findings allow control of the feature sizes, and nodular domains with diameters well below 50 nm were produced. Films prepared with dyes possessing a mobile counterion were always unstable. To rationalize the findings, we developed a thermodynamic model showing that electrostatic forces induced by the mobile counterions act as destabilizing pressure.

Introduction

Spin coating is often used to create uniform films of organic small molecules and polymers. For example, organic light-emitting diodes or all-organic photovoltaic devices are fabricated widely by this method. Therefore, the understanding of instabilities in thin liquid films is attracting attention arising for both scientific and technological reasons.[1]

The mechanisms leading to film rupture and dewetting can be of different natures and depend on the particular boundary conditions. One source of instability is induced by convective flows driven by evaporation of solvent during spin coating. These Marangoni instabilities are caused by either local cooling at the surface or concentration inhomogeneities.[2–4] When the film is thin enough (below ∼100 nm), the stability is determined by van der Waals or electrostatic interactions between the film surface and substrate.[5–7]

Similarly, a blend system that initially phase-separates into a bilayer can destabilize by liquid−liquid dewetting. This situation is more complicated since the dynamics of two coupled deformable interfaces is involved. Obviously, a bilayer system shows a greater variety of dewetting pathways than a single layer. The conditions that promote a greater destabilization of one of the two layers determine which layer ruptures first. The first initiation of rupture mainly determines the long-run appearance of dewetted structures. A two-layer system with a much thicker lower liquid layer has been modeled in ref 8. The initial phases of bilayer instabilities have been studied numerically in refs 9 and 10, and these studies of the linear stages of instabilities were extended toward the subsequent, nonlinear regime.[11–14] Other models describe a system which also contains surfactants[15–17] and includes solvent evaporation.[18–20] Most experimental work has been performed on polymer bilayer systems. These experiments have indeed shown a richer variety of mesoscale morphologies compared to those on single-layer films.[21–30] Droplet formation in a film from a binary solution of

* To whom correspondence should be addressed. (J.H.) Phone: +41 44 823 4356. Fax: +41 44 823 4012. E-mail: jakob.heier@empa.ch. (J.G.) Phone: +31 30 253 5000. Fax: +31 30 253 3870. E-mail: j.groenewold@uu.nl.

† EMPA.

‡ University of Utrecht.

(1) Oron, A.; Davis, S. H.; Bankoff, S. G. *Rev. Mod. Phys.* **1997**, *69*, 931–980.
(2) Scriven, L. E.; Sternling, C. V. *Nature* **1960**, *187*, 186–188.
(3) Pearson, J. R. A. *J. Fluid Mech.* **1958**, *4*, 489–500.
(4) Haas, D. E.; Birnie, D. P., III *J. Mater. Sci.* **2002**, *37*, 2109–2116.
(5) Maldarelli, C.; Jain, R. K. In *Thin Liquid Films: Fundamentals and Applications*; Ivanov, I. B., Ed.; Marcel Dekker: New York, 1988; p 497.
(6) Israelachvili, J. N. *Intermolecular and Surface Forces*, 2nd ed.; Academic Press: London, 1992.
(7) Hunter, R. J. *Foundation of Colloid Science*; Clarendon Press: Oxford, 1992; *Vol. 1*.
(8) Brochard Wyart, F.; Martin, P.; Redon, C. *Langmuir* **1993**, *9*, 3682–3690.
(9) Pototsky, A.; Bestehorn, M.; Merkt, D.; Thiele, U. *Phys. Rev. E* **2004**, *70*, 025201.
(10) Bandyopadhyay, D. Stability and dynamics of bilayers. Master Thesis, Department of Chemical Engineering, Indian Institute of Technology Kanpur, 2001.
(11) Pototsky, A.; Bestehorn, M.; Merkt, D.; Thiele, U. *J. Chem. Phys.* **2005**, *122*, 224711.
(12) Bandyopadhyay, D.; Gulabani, R.; Sharma, A. *Ind. Eng. Chem. Res.* **2005**, *44*, 1259–1272.
(13) Bandyopadhyay, D.; Sharma, A. *J. Chem. Phys.* **2006**, *125*, 054711.
(14) Pototsky, A.; Bestehorn, M.; Merkt, D.; Thiele, U. *Europhys. Lett.* **2006**, *74*, 665–671.
(15) Zhang, Y. L.; Matar, O. K.; Craster, R. V. *J. Colloid Interface Sci.* **2003**, *262*, 130–148.
(16) Craster, R. V.; Matar, O. K. *J. Fluid Mech.* **2000**, *425*, 235–258.
(17) Matar, O. K.; Craster, R. V.; Warner, M. R. E. *J. Fluid Mech.* **2002**, *466*, 85–111.
(18) Danov, K. D.; Paunov, V. N.; Alleborn, N.; Raszillier, H.; Durst, F. *Chem. Eng. Sci.* **1998**, *53*, 2809–2822.
(19) Danov, K. D.; Paunov, V. N.; Stoyanov, S. D.; Alleborn, N.; Raszillier, H.; Durst, F. *Chem. Eng. Sci.* **1998**, *53*, 2823–2837.
(20) Paunov, V. N.; Danov, K. D.; Alleborn, N.; Raszillier, H.; Durst, F. *Chem. Eng. Sci.* **1998**, *53*, 2839–2857.
(21) de Silva, J. P.; Geoghegan, M.; Higgins, A. M.; Krausch, G.; David, M.-O.; Reiter, G. *Phys. Rev. Lett.* **2007**, *98*, No. 267802.
(22) Higgins, A. M.; Jones, R. A. L. *Nature* **2000**, *404*, 476–478.
(23) Lin, Z.; Kerle, T.; Baker, S. M.; Hoagland, D. A.; Schäffer, E.; Steiner, U.; Russell, T. P. *J. Chem. Phys.* **2001**, *114*, 2377–2381.
(24) Lin, Z.; Kerle, T.; Russell, T. P.; Schäffer, E.; Steiner, U. *Macromolecules* **2002**, *35*, 3971–3976.
(25) Lin, Z.; Kerle, T.; Russell, T. P.; Schäffer, E.; Steiner, U. *Macromolecules* **2002**, *35*, 6255–6262.
(26) Lambooy, P.; Phelan, K. C.; Haugg, O.; Krausch, G. *Phys. Rev. Lett.* **1996**, *76*, 1110–1113.
(27) Pan, Q.; Winey, K. I.; Hu, H. H.; Composto, R. J. *Langmuir* **1997**, *13*, 1758–1766.

10.1021/la800099j CCC: $40.75
Published on Web 06/12/2008

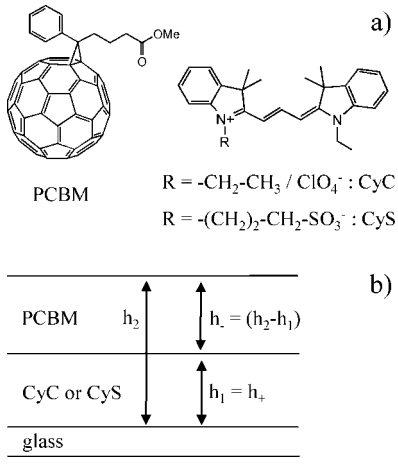

Figure 1. (a) Molecular structures of the soluble fullerene derivative PCBM and the cyanine dyes CyC with the free counteranion ClO_4^- and CyS with the covalently linked SO_3^- anion. (b) Diagram that indicates the relevant thicknesses in the transient bilayers formed during spin coating.

small molecules during solvent evaporation has been reported recently.[31,32]

Here, we present our finding that spin coating mixtures of ionic cyanine dyes and [6,6]-phenyl-C_{61}-butyric acid methyl ester (PCBM; a soluble derivate of C_{60}) leads to the formation of a rich variety of phase-separated morphologies which we attribute to liquid−liquid dewetting processes. During spin coating a transient bilayer is formed, with the dye solution wetting the substrate and the PCBM solution forming a layer on top of that. Upon evaporation of the remaining solvent, the film thins and the interfaces destabilize. The final film consists of coexisting domains of PCBM and cyanine dye, which were imaged with atomic force microscopy (AFM). We investigated the different morphologies that occur as a function of composition and film thickness and discuss the driving forces responsible for film destabilization. We explain a transition from rupture in the top layer to rupture in the bottom layer and the secondary events that follow the initial film rupture leading to the final film morphology.

Experimental Section

PCBM was purchased from Solenne B.V., The Netherlands. The cyanine dyes 1,1′-diethyl-3,3,3′,3′-tetramethylcarbocyanine perchlorate (CyC) and 1-sulfopropyl-1′-ethyl-3,3,3′,3′-tetramethylcarbocyanine (CyS) were synthesized based on published procedures.[33,34] The chemical structures of the materials are shown in Figure 1. PCBM, CyC, and CyS were dissolved in the common solvent chlorobenzene (CB), chloroform (CF), or tetrachloroethane (TCE) and then spin coated onto glass substrates. Thicknesses were adjusted by varying the concentration and spin speed. PCBM was selectively removed by immersing the samples in hexane for up to 3 min in an ultrasonic bath. CyC and CyS were selectively removed by immersing the samples in 2,2,3,3-tetrafluoropropanol (TFP) for ∼3 s.

AFM measurements were performed on a Nanosurf Mobile S in tapping mode at a resonance frequency of 170 kHz. We used rectangular silicon cantilevers (Mikromasch, Nanosensors) with a typical force constant of ∼40 N m^{-1} and a tip radius of curvature of ∼10 nm. Samples were analyzed using WsXM scanning probe microscopy software.[35] Final average film thicknesses were determined with UV−vis spectroscopy. A precisely determined film area was dissolved in CB and diluted to a maximum absorbance of about 0.8. Absorption spectra of these solutions were a superposition of the typical PCBM peak around 330 nm and the peak of the cyanine monomers at ∼559 nm. The spectra were fitted to the absorption spectra of solutions of the individual components obtained from films with known thicknesses determined by AFM. Absorption spectra were measured on a Varian Cary 50 UV−vis spectrophotometer. UV−vis spectroscopy was also employed to prove the complete removal of either component from the film using the selective solvent hexane or TFP.

Surface energies of the solid films were obtained from the advancing contact angles of droplets of different liquids after the method of Owens, Wendt, Rabel, and Kaelble.[36,37] For the glass substrate we used the liquids water, glycerol, formamide, and diiodomethane. For CyC, CyS, and PCBM the liquids water, *cis*-decalin, *n*-hexane, and glycerol were used. In that case the choice of fluids was rather limited, as they must not dissolve the organic material during the measurement.

X-ray photoelectron spectroscopy (XPS) was used to prove that ClO_4^- ions originating from the cyanine dye reside within the PCBM phase. Typically, a surface layer of 2−3 nm depth was scanned. Measurements were performed on a PHI-Quantum 2000 "imaging XPS" instrument with a monochromatic Al Kα X-ray source. The vacuum in the measurement chamber was kept below 5×10^{-7} Pa. During the measurement the surface was continuously neutralized with low-energy electrons and Ar ions. On all samples a survey scan and detailed spectra of the C1s reference line and Cl2p line were taken.

Results

Figure 2 shows a rich variety of phase-separated morphologies for spin-coated blend films of PCBM and CyC. To identify the phases in detail, the components were removed with selective solvents. The left column shows AFM scans of the original films; the images of the CyC and PCBM phases alone are shown in the middle and right columns, respectively. As-prepared samples revealed characteristic topographical structures of laterally separated domains, and the complementary scans allowed construction of a complete picture of phase morphologies within the films. The patterns were tentatively classified in five categories of typical morphologies (Figure 3). As shown below, this classification is reasonable, because the morphology types are almost independent of the total thickness, and the film height only determines the length scales of the domain features.

For low PCBM fractions, almost flat films with scattered indentations were observed (Figure 2a, left). Only after removal of PCBM did the recesses become more pronounced, indicating that each hole was filled with PCBM (Figure 2a, middle). Removal of the entire CyC matrix indeed revealed a network of individual PCBM domains (Figure 2a, right). We confirmed with UV−vis spectroscopy that during the removal of the CyC matrix almost no PCBM was washed away. This particular film is thus composed of scattered PCBM domains within a continuous matrix of CyC. PCBM domains that are close enough to the top surface leave sinkholes in the CyC layer (Figure 3A).

With increasing fullerene content, the film morphology changed to layered PCBM domains of varying packing density, extending

(28) Segalman, R. A.; Green, P. F. *Macromolecules* **1999**, *32*, 801–807.
(29) Wang, C.; Krausch, G.; Geoghegan, M. *Langmuir* **2001**, *17*, 6269–6274.
(30) Kang, H.; Lee, S. H.; Kim, S.; Char, K. *Macromolecules* **2003**, *36*, 8579–8583.
(31) Govor, L. V.; Parisi, J.; Bauer, G. H.; Reiter, G. *Phys. Rev. E* **2005**, *71*, 051603.
(32) Govor, L. V.; Reiter, G.; Bauer, G. H.; Parisi, J. *Phys. Lett. A* **2006**, *353*, 198–204.
(33) Ernst, L. A.; Gupta, R. K.; Mujumdar, R. B.; Waggoner, A. S. *Cytometry* **1989**, *10*, 3–10.
(34) Wang, J.; Cao, W. -F.; Su, J.- H.; Tian, H.; Huang, Y.-H.; Sun, Z. -R. *Dyes Pigm.* **2003**, *57*, 171–179.
(35) Horcas, I.; Fernández, R.; Gómez-Rodríguez, J. M.; Colchero, J.; Gómez-Herrero, J.; Baro, A. M. *Rev. Sci. Instrum.* **2007**, *78*, 013705.
(36) Owens, D. K.; Wendt, R. C. *J. Appl. Polym. Sci.* **1969**, *13*, 1741–1747.
(37) Kaelble, D. H. *J. Adhes.* **1970**, *2*, 66–81.

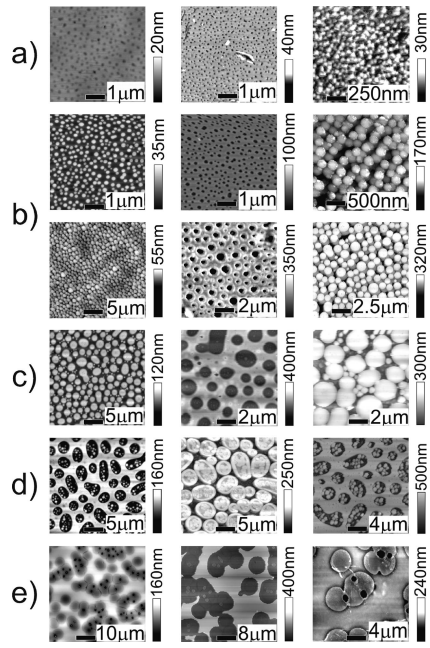

Figure 2. Morphologies of PCBM−CyC films spin coated on glass from chlorobenzene solution with different weight ratios of PCBM to CyC. The left column shows the films as spin coated, the middle column presents the films after PCBM removal, and the right column shows the films after CyC removal. The fraction of PCBM increases from the top to the bottom. The average total film thickness (h_2) and $r = (h_2 - h_1)/h_1$, the ratio of the average PCBM thickness to the average CyC thickness (h_1) are (a) $h_2 = 14$ nm and $r = 0.16$, (b) $h_2 = 70$ nm and $r = 1.0$ and $h_2 = 150$ nm and $r = 0.8$, (c) $h_2 = 330$ nm and $r = 1.1$, (d) $h_2 = 208$ nm and $r = 1.9$, and (e) $h_2 = 186$ nm and $r = 2.8$.

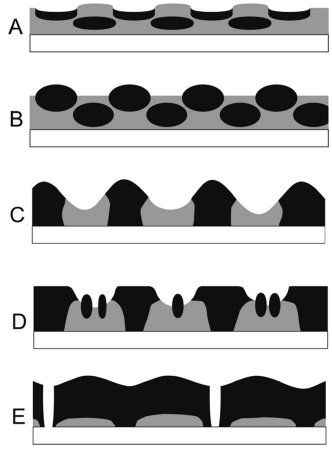

Figure 3. Schematic diagram of the main categories of dewetting patterns identified in the PCBM−CyC system. Panels A−E refer to the AFM images shown in panels a−e of Figure 2. With increasing PCBM (black) content, the morphology transforms from isolated PCBM domains in a CyC (gray) matrix into a bilayer system, with PCBM against the vacuum interface and CyC against the substrate interface.

above the CyC surface layer (Figures 2b and 3B). Increasing the PCBM content further forms a layer of laterally fully separated PCBM domains within CyC. The PCBM domains extend from the substrate until above the CyC matrix surface level (Figures 2c and 3C). One common structural feature for films with PCBM to CyC thickness ratios between ∼0.1 and ∼1 is therefore that PCBM decomposes into individual domains arranged within a film-forming, continuous CyC matrix (Figure 3A−C).

For even higher PCBM fractions, a stability transition occurs and PCBM switches from the domain-forming minority component to the film-forming majority component (Figure 2d and

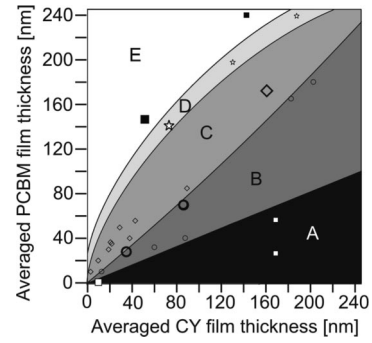

Figure 4. Morphology classification of PCBM−CyC films according to average film thicknesses as determined by UV−vis spectroscopy. Each symbol represents an experimental data point. Morphologies A (empty squares), B (circles), C (tilted squares), D (stars), and E (filled squares) correspond to the morphology types of parts a−e of Figure 2 and the generalized pictures A−E of Figure 3, respectively. The larger symbols indicate the actual samples shown in Figure 2. This diagram indicates that it is mainly the ratio of the PCBM thickness to the CyC thickness which determines the type of morphology.

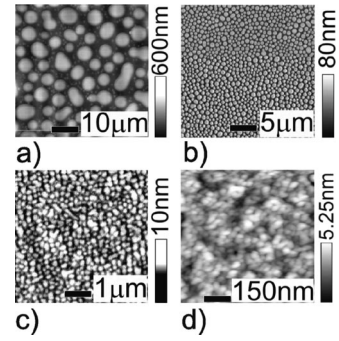

Figure 5. PCBM−CyC samples with similar types of morphology (morphology C in Figure 3), but different film thicknesses. The size of the domains depends critically on the film thickness and varies by more than 2 orders of magnitude. Key (h_2 = average total thickness; r = ratio of the average PCBM thickness to the average CyC thickness): (a) $h_2 = 594$ nm, $r = 1.2$; (b) $h_2 = 57$ nm, $r = 1.6$; (c) $h_2 = 12$ nm, $r = 2.9$; (d) $h_2 = 2$ nm, $r = 2.5$.

3D). The PCBM domains merge into a bicontinuous surface layer, and CyC now forms isolated domains. Holes in the PCBM layer form exclusively above CyC pillars, and these are populated with small PCBM domains. Finally, a double-layer system is established (Figures 2e and 3E); a thick PCBM layer forms on top of CyC, and both layers show dewetting holes.

Figure 4 summarizes in a schematic phase diagram the compositions of the main morphology types identified so far. Similar morphologies develop for films with similar thickness ratios of PCBM to CyC. The absolute thickness of each layer is less important for the type of morphology that develops. This indicates that the structure-directing mechanisms originate from interactions between the film surfaces. Within one "phase" the lateral dimensions decrease with decreasing film thickness, indicating that the strength of the destabilization force increases for thinner films.

This is illustrated in Figure 5 showing AFM images of films with decreasing total thickness, but all with morphology type C. The thickness ratio of PCBM to CyC varied between 1.2 and 2.9, but we still stayed within the same morphology range (see Figure 4). The characteristic wavelengths decrease with decreasing film thickness, while the surface coverage of the PCBM domains increases. The diameters of the domains change over more than 2 orders of magnitude. This is further quantified in Figure 6 by plotting the dominant lateral wavelength of the domains over the

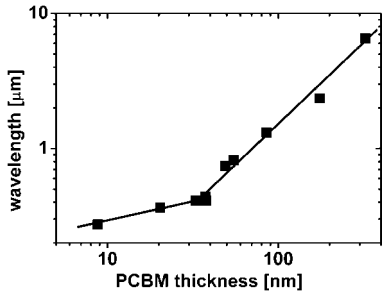

Figure 6. Dependence of the dominant instability wavelength on the average PCBM film thickness. The analysis was performed on films with morphology type C. The wavelength was obtained from maxima in the power spectral density from the AFM images. A transition in the critical exponent occurs: a least-squares linear fit to PCBM thicknesses below 30 nm reveals a scaling exponent of 0.30; for PCBM thicknesses larger than 30 nm, the scaling exponent is 1.18.

PCBM thickness for the morphologies as depicted in Figures 2c and 5. We found morphology C most suitable to perform the analysis because that morphology shows a clear lateral separation of the domains. Assuming a negligible influence of the different relative CyC layer thicknesses on the PCBM dewetting behavior, a critical exponent of 1.18 was found for films thicker than ~30 nm, which almost suggests a linear dependence of the domain size on film thickness. For PCBM films below 30 nm the scaling exponent drops to 0.3 as shown in Figure 6. An explanation of the origin of the instability should then also account for the observed thickness dependence. The image shown in Figure 5d is not included in the analysis as we could not identify a clear dominant wavelength from the Fourier analysis of the image.

Discussion

The experimental results suggest that film formation proceeds via a transient bilayer[9,38] during spin coating, with a CyC film at the solution−substrate interface and a PCBM film at the solution−air interface. The PCBM solution can wet a layer of CyC solution if the condition for the spreading coefficient $S_{21} = \gamma_1 - \gamma_2 - \gamma_{21} > 0$ is fulfilled.[39] γ_2, γ_1, and γ_{21} denote the surface tensions of the PCBM solution with air, the CyC solution with air, and between the PCBM and CyC solutions, respectively. With $\gamma_{21} = \gamma_2 + \gamma_1 - 2(\gamma_1\gamma_2)^{1/2}$, S_{21} is positive as long as $\gamma_2 < \gamma_1$.[6] In that case, the formation of a PCBM layer at the air surface minimizes the free energy at the interface between air and the solution.[40] The bilayers at the beginning of spin coating are composed of dilute PCBM and CyC solutions with surface tensions just slightly lower and higher than the value $\gamma_{CB} = 32.99$ mN m^{-1} of chlorobenzene,[41] and γ_2 and γ_1 develop during evaporation in opposite directions to $\gamma_{PCBM} = 23.9$ mN m^{-1} and $\gamma_{CyC} = 34.3$ mN m^{-1} of the pure materials (Table 1). Therefore, the condition $S_{21} > 0$ holds probably for the entire evaporation process, even when one component solidifies faster than the other one. The surface tension for PCBM differs slightly from the value reported earlier.[42] This can be easily accounted for by differences in the measurement method.

Direct evidence for the bilayer-type film structure can be most easily found in asymmetric films as shown in Figure 7. Here, the much thicker PCBM layer dewetted on a larger length scale from the bottom CyC layer, leaving a smooth cyanine surface. This picture also confirms the importance of the PCBM layer for interface destabilization: the blank CyC surface is flat, while the surface originally covered by PCBM shows a destabilized interface.

Film instabilities manifest themselves in a magnification of interface fluctuations followed potentially by rupture. In Figure 8 we propose sequences leading to the final morphologies as observed in Figure 2. Characteristic of thin-film instabilities in general is that thin layers destabilize on a shorter time scale than

Table 1. Experimental Values of Surface Tensions, Calculated Hamaker Constants, and Results of XPS Measurements

		Hamaker constant A [a] (10^{-20} J)			XPS		
	surface tension γ (mN m^{-1})		CyC[b]	CyS[b]		PCBM[d]	PCBM−CyC[e]
glass	64.46	A_{g21s}[c]	−2.18	0.10	Cl2p[f]	0.2	0.4
CyC	34.30	A_{21s}	−0.43	0.07	ClO_4^- [g]	0	12.4
CyS	66.10	$A_{12\,g}$	−0.97	−3.25	Cl[g]	100	87.6
PCBM	23.90						

[a] Calculated with $A_{ii} = 24\pi\gamma_i D^2$, $D = 0.165$ nm, $A_{ijkl} = (\sqrt{A_{ll}} - \sqrt{A_{kk}})(\sqrt{A_{ii}} - \sqrt{A_{jj}})$, and $A_{ijk} = (\sqrt{A_{ii}} - \sqrt{A_{jj}})(\sqrt{A_{kk}} - \sqrt{A_{jj}})$. [b] Layer systems air−PCBM−CyC−glass and air−PCBM−CyS−glass. [c] Subscripts g = gas (air), 2 = PCBM layer, 1 = cyanine layer, and s = glass substrate. [d] Pure PCBM layer. [e] PCBM−CyC blend film measured after removal of CyC. [f] Concentration (atom %) of chlorine with respect to carbon. [g] Deconvolution of total chlorine content Cl2p into fractions (%) of perchlorate (ClO_4^-) and other chlorine-containing components (Cl).

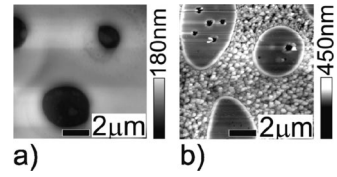

Figure 7. AFM images of a PCBM−CyC film where a thick PCBM layer (average thickness 440 nm) covers a thinner CyC layer (180 nm) as spin coated (a) and after removal of PCBM (b). This sample can be approximately assigned to morphology type E. The PCBM layer dewetted locally on a micrometer length scale from the bottom CyC layer (dark circles visible in (a)). Removal of the fullerene (b) reveals a roughened CyC surface for regions that were covered by PCBM; however, the dewetted CyC regions forming an air−CyC interface flattened out again in (b), because CyC alone wets the glass substrate.

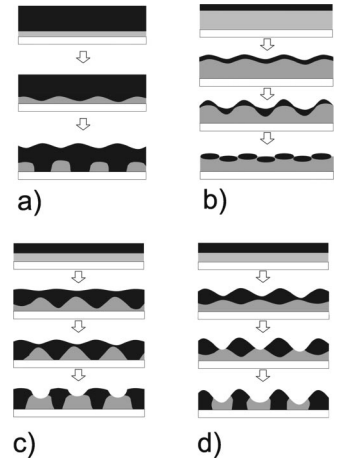

Figure 8. Diagram showing how different morphologies evolve from different thickness ratios of a destabilizing PCBM−CyC double layer. (a) and (b) present asymmetric films where the top PCBM layer is much thicker than the base CyC layer (a) or contrariwise (b). Film rupture always occurs in the thinner layer. (c) and (d) show symmetric films. Here both layers rupture, and in (c) initial film rupture occurs in the bottom layer, while in (d) initial film rupture occurs in the top layer.

(38) Heriot, S. Y.; Jones, R. A. L. *Nat. Mat.* **2005**, *4*, 782–786.
(39) Adamson, A. W. H. *Physical Chemistry of Surfaces*; Wiley: New York, 1982.
(40) Bruder, F.; Brenn, R. *Phys. Rev. Lett.* **1992**, *69*, 624–627.
(41) Lide, D. R. *Handbook of Organic Solvents*; CRC Press, Inc.: Boca Raton, FL, 1995.
(42) Nilsson, S.; Bernasik, A.; Budkowski, A.; Moons, E. *Macromolecules* **2007**, *40*, 8291–8301.

thicker layers.[9] Figure 8a depicts this situation for a thin CyC film that develops into a typical morphology as found in Figure 2e. In addition, the interfaces can destabilize in-phase (called the bending mode) or out-of-phase (the squeezing mode), and the actual mode is critically dependent on layer thicknesses, surface energies, or viscosities.[8] In Figure 8b, individual PCBM domains develop from a bending mode in the valleys and peaks of the top layer.

For films with comparable layer thicknesses, modulations of relevant amplitudes can develop in both layers, and interpenetration of one layer into the other will locally also decrease that layer thickness, which favors rupture. Parts c and d of Figure 8 depict the two situations, where squeezing mode destabilizations lead finally to domains separated by valleys. In Figure 8c, rupture first occurs in the bottom layer. Experimentally, this is realized in samples as shown in Figure 2d. In Figure 8d the complementary situation is drawn; here, rupture occurs first in the top layer, and rather regularly spaced and shaped droplets are formed. In the second step the PCBM domains penetrate the lower layer, which will promote its instability. The bottom layer ruptures as well, and as a consequence, the PCBM domains fully penetrate the lower layer and make contact with the glass substrate. Penetration of an upper layer into a lower layer is an experimentally well established phenomenon at soft interfaces.[26] Experimentally, this scenario is observed for samples shown in Figures 2c and 5. Common to all scenarios of Figure 8 is the formation of a long-range primary surface wave pattern that determines the principal wavelength; at the moment of film breakup, a cascade of secondary local events become more important and determine the ultimate phase-separated morphology.

As explained above, the interfacial tensions alone suggest stable bilayer PCBM−CyC films; thus, additional forces able to amplify fluctuations and leading to spinodal dewetting are operative. We first discuss van der Waals forces. These interactions are omnipresent and are known to affect the stability of thin films. The system is described as a two-layer system sandwiched between a solid substrate and a gas, assuming that almost all solvent has evaporated. The interfacial energy contains three contributions:[6]

$$\Delta G_{\mathrm{vw}} = -\frac{A_{\mathrm{g21s}}}{12\pi h_2^{\,2}} - \frac{A_{\mathrm{21s}}}{12\pi h_1^{\,2}} - \frac{A_{\mathrm{12g}}}{12\pi (h_2 - h_1)^2} \qquad (1)$$

h_2 denotes the total film thickness and h_1 the thickness of the cyanine layer (Figure 1). A_{g21s}, A_{21s}, and A_{12g} are four- and three-index Hamaker constants, with the subscripts s, 1, 2, and g referring to the substrate (glass), liquid 1 (cyanine), liquid 2 (PCBM), and the gas (air), respectively. These constants correspond to the interactions of air with glass across the organic layers, of the PCBM layer with glass across the cyanine layer, and of the cyanine layer with air across PCBM.

The two-layer film is unstable if the energy surface $\Delta G_{\mathrm{vw}}(h_1,h_2)$ as a function of the film thicknesses is concave or has a saddle point. This corresponds to the condition[11]

$$\det \Delta G_{\mathrm{vw}} = (\partial^2_{h_1h_1}\Delta G_{\mathrm{vw}})(\partial^2_{h_2h_2}\Delta G_{\mathrm{vw}}) - (\partial^2_{h_1h_2}\Delta G_{\mathrm{vw}})^2 < 0 \qquad (2)$$

or

$$\partial^2_{h_1h_1}\Delta G_{\mathrm{vw}} < 0 \qquad (3)$$

The individual Hamaker constants can be determined from the experimentally determined surface tensions γ_i as $A_{ii} = 24\pi\gamma_i D^2$, where D is the cutoff intermolecular separation, $D = 0.165$ nm.[6]

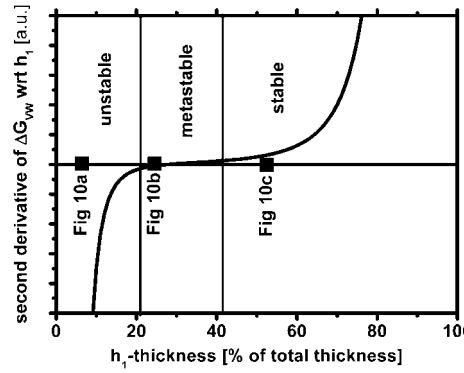

Figure 9. Calculated shape of the second derivative of the free energy ΔG_{vw} with respect to the CyS cyanine layer thickness h_1 (eq 3). For low CyS portions, the film is unstable, and with increasing CyS content the film passes through a metastable to a stable regime. The squares mark the experimental thickness ratios of samples shown in Figure 10.

From there the effective Hamaker constants were approximated with the individual constants[43,44] as $A_{ijkl} = (\sqrt{A_{ll}} - \sqrt{A_{kk}})(\sqrt{A_{ii}} - \sqrt{A_{jj}})$ and $A_{ijk} = (\sqrt{A_{ii}} - \sqrt{A_{jj}})(\sqrt{A_{kk}} - \sqrt{A_{jj}})$. Depending on the sign of the Hamaker constants, the disjoining pressure can be attractive or repulsive, leading to film destabilization or stabilization.

For the PCBM−CyC system all Hamaker constants are negative (Table 1), which implies unconditionally stable layers over the entire composition and thickness range. The exact determination of the Hamaker constants is debatable, but even a large variation of the experimentally determined values did not alter the physical picture. Therefore, van der Waals forces do not explain the experimental fact that PCBM−CyC thin films always were unstable. The situation is different for the second system where a blend of PCBM with the cyanine dye CyS was investigated (Figure 1). The two cyanines differ in their surface tensions (Table 1); still, a transient bilayer is formed during the initial stages of spin coating. The Hamaker constants A_{g21s} and A_{21s} are positive, while $A_{\mathrm{12\,g}}$ is negative (Table 1). Therefore, the conditions for film stability for the PCBM−CyS system vary with varying thicknesses h_2 and h_1. Figure 9 displays the quantitative course of the stability condition of eq 3. Accordingly, a film with a very low CyS thickness compared to PCBM thickness will destabilize via van der Waals forces. Increasing the CyS fraction leads to metastable and finally to stable film configurations. The other stability condition, eq 2, is always positive, and has not been included in Figure 9.

The prediction of Figure 9 could be readily realized experimentally. Figure 10 displays AFM scans of PCBM−CyS films with compositions in the unstable, metastable, and stable regions. Different from CyC, the CyS system follows precisely the predictions expected for van der Waals destabilizing forces. For both PCBM−cyanine systems, we thus tentatively exclude Marangoni-type convection flows that drive the bilayer instability or a primary phase separation process as reported for a PCBM−polymer−solvent system[42] and favor interfacial forces.

The fundamental difference between the two cyanines is that in the case of CyC the anion is free, while for CyS the anion is covalently linked to the chromophore. This could give rise to electrostatic forces in thin CyC films, and space charge could build up, for example, by transfer of ClO_4^- across the interface

(43) Visser, J. *Adv. Colloid. Interface Sci.* **1972**, *3*, 331–363.
(44) Bargeman, D.; van Voorst Vader, F. *J. Electroanal. Chem. Interfacial Electrochem.* **1972**, *37*, 45–52.

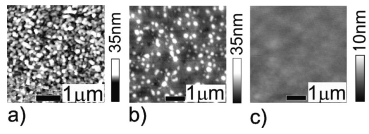

Figure 10. Morphologies of PCBM−CyS films with total film thicknesses h_2 and thickness ratios r of PCBM to CyS: (a) $h_2 = 28$ nm, $r = 14$; (b) $h_2 = 16$ nm, $r = 3.1$; (c) $h_2 = 103$ nm, $r = 0.81$. The film in (a) with the smallest CyS thickness compared to the PCBM thickness shows a spinodal destabilization pattern. An increase of the relative CyS thickness results in a stable bilayer system (c) as confirmed by measuring the thickness of the CyS film after PCBM removal with AFM. Panel b can be directly compared to Figure 5c because both films have the same thickness. PCBM forms droplets on top of both cyanine films. On CyC, a spinodal dewetting pattern of PCBM is observerd, whereas a preferred wavelength is not present in the case of CyS. In addition, PCBM dewets on CyC on a much smaller length scale. This suggests a spinodal dewetting process for the PCBM−CyC film, but nucleation and growth for the PCBM−CyS film. Since CyS is poorly soluble in chlorobenzene, we use the solvent tetrachloroethane for the thickest cyanine film. Therefore, the results shown in (c) should be interpreted with some care.

into the PCBM-rich phase of the solution (see below).[45–47] A result of this process is a net negative charge residing in the PCBM layer and a net positively charged CyC layer.

It is interesting to calculate the role of net charge in the free film energy. Coulomb interactions have a long range unless there is screening by unbound ion pairs. This range is given by the Debye length, which is inversely proportional to the square root of the concentration of free ion pairs.[48,49] As the dissociation energy of ionic species in an organic matrix is usually very high, we will assume that the Debye length is larger than the thickness of the CyC or PCBM film. This assumption implies that we model the two-component film by charges that interact via unscreened Coulomb interactions. The role of charge in phase-separating fluid systems can be found in a wide variety of systems including nuclear physics,[50] colloids,[51,52] and fluid systems containing space charge.[53]

We consider the situation of two planar films. The bottom CyC film is positively charged with charge density ρ_+, dielectric constant ε_+, and thickness h_+. On top we have the negatively charged PCBM film with charge density ρ_-, dielectric constant ε_-, and thickness h_-. For simplicity we assumed that the individual charge densities are constant throughout the domains. This assumption can in certain cases introduce errors of 10−50%, but it does not change the order of magnitude of the electrostatic free energy.

The electrostatic energy pertaining to the two-layer model with uniform charge forms the basis for the intrinsic thin-film instability of interest. Under a wide variety of circumstances it can be shown that the electrostatic contribution is more important for the instability than the van der Waals force. The electrostatic energy E of the two-layer film system with area A is given by

$$\frac{E}{A} = \frac{1}{6}\left[\frac{\rho_+{}^2 h_+{}^3}{\varepsilon_+} + \frac{\rho_-{}^2 h_-{}^3}{\varepsilon_-}\right] \tag{4}$$

This expression contains the dependence on the film thicknesses of the layers. Similar to the case of van der Waals forces (see above), driving forces for film instabilities are typically proportional to the second derivative of the energy per unit area with respect to h_+ or h_- or a combination of these. It is interesting to note that the second derivative of this energy with respect to the thicknesses is always positive and therefore does not lead to instability. This is typically the case if the charge transfer is so slow that the charge density of the domains remains constant. This is the case for instance if the counterions are bound (such as in CyS).

The situation is radically different if the charges can easily migrate from one domain to the other. This way the charge densities are no longer constant if an undulation of one (or two) of the film thicknesses occurs. Because the charge densities are determined by transfer of ions from the CyC to the PCBM layer one has by charge neutrality

$$\rho_+ h_+ = \rho_- h_- = \sigma \tag{5}$$

With this condition the charge densities can be eliminated from the expression for the electrostatic energy to give

$$\frac{E}{A} = \frac{\sigma^2}{6}\left[\frac{h_+}{\varepsilon_+} + \frac{h_-}{\varepsilon_-}\right] \tag{6}$$

In addition to this electrostatic contribution to the energy, we must also invoke a free energy of transfer associated with the migration of a counterion from the CyC domain to the PCBM domain. Specific interactions between the counterion and PCBM in combination with a gain in entropy can lead to a spontaneous process of counterion transfer. Presently we can only speculate about the microscopic mechanism for the apparent affinity of the chlorate ions with the PCBM phase. Possible mechanisms may involve solvation, whereby the ions in the solution are complexed by solvent molecules. For simplicity, this transfer is assumed to be associated with a free energy gain ΔW per charge, thereby neglecting possible concentration effects. Then the total (free) energy F for the two-layer system is

$$\frac{F[\sigma]}{A} = \frac{\sigma^2}{6}\left[\frac{h_+}{\varepsilon_+} + \frac{h_-}{\varepsilon_-}\right] - \Delta W\frac{\sigma}{e} \tag{7}$$

Here e is the value in Coulomb for an elementary charge such that σ/e is equal to the number of transferred charges per unit area. With this free energy the number of transferred charges per unit area can be obtained by minimization with respect to σ. This minimization leads to the following realization of the charge density σ_*:

$$\sigma_* = \frac{3}{e}\frac{\Delta W}{h_+/\varepsilon_+ + h_-/\varepsilon_-} \tag{8}$$

This expression is a manifestation of the fact that the transfer of ions from CyC to PCBM is limited by the Coulomb repulsions that are invariably associated with this transfer. Reinserting this optimal value in the free energy expression (eq 7), the following result is found:

$$\frac{F}{A} = -\frac{3}{2e^2}\frac{\Delta W^2}{h_+/\varepsilon_+ + h_-/\varepsilon_-} \tag{9}$$

Inspecting the second derivative of this expression, it can be concluded that this free energy always leads to instability, as the second derivative is invariably negative. This does not mean of course that any film must be unstable as we have made a number of assumptions, of which the most important are (i) no screening of the Coulomb interaction, i.e., the number of free ion pairs is negligible, and (ii) sufficient mobility of the counterions to migrate from PCBM and CyC domains.

(45) Nüesch, F.; Faes, A.; Zuppiroli, L.; Meng, F.; Chen, K.; Tian, H. *J. Mater. Sci.* **2005**, *40*, 1353–1357.
(46) Demchuk, M. I.; Ishchenko, A. A.; Mikhailov, V. P.; Avdeeva, V. I. *Chem. Phys. Lett.* **1988**, *144*, 99–103.
(47) Benmansour, H.; Castro, F. A.; Nagel, M.; Heier, J.; Hany, R.; Nüesch, F. *Chimia* **2007**, *61*, 787–791.
(48) Derjaguin, B. V.; Landau, L. D. *Acta Physicochim. URSS* **1941**, *14*, 633–652.
(49) Verwey, E. J. W.; Overbeek, J. T. G. *The Theory of the Stability of Lyophobic Colloids*; Elsevier: Amsterdam, 1948.
(50) Baym, G.; Bethe, H.; Pethick, C. *Nucl. Phys. Ser. A* **1971**, *175*, 225–271.

The instability hidden in eq 9 can be understood as follows: If an undulation takes place, one region of the film becomes narrower, yet another region becomes thicker. If the charges are immobile, then the narrow regions get a higher charge density and the thicker regions get a smaller density. In the case of mobile ions however the charge densities adapt to a more uniform value due to charge transfer in the thick regions and recombination in the narrow regions. The net result is, however, more dissociation than recombination, which means a lower total free energy.

XPS finally proved that ClO_4^- anions were present in the PCBM phase (Table 1). Pure PCBM films were compared with results from mixed PCBM−CyC films of morphology type C (Figure 3) after selective dissolution of the dye. For pure PCBM, ClO_4^- was not present, and the chlorine detected originated from small amounts of residual solvent chlorobenzene (Table 1). For mixed films, the total chlorine content doubled and the perchlorate fraction increased to 12.4%. That the ClO_4^- anions present are accompanied by the dye chromophore can be excluded: a UV−vis spectrum of the dissolved PCBM phase did not reveal any CyC signature, while a comparison solution with the same ClO_4^- fraction, but now accompanied by the dye, showed a clear CyC peak. This result suggests that CyC molecules were not trapped in the fullerene matrix and therefore readily dissolved.

Calculating the amount of perchlorate with respect to carbon from the XPS measurements (Table 1), one obtains 1 chlorate ion/28 PCBM molecules. Such a concentration of chlorate ions is about 100 times higher compared to an estimate based on eq 8. Thereby, we assumed a free energy gain per charge $\Delta W =$ 1 eV and took the final film thickness. Even given the error bars, crudeness of the model, and uncertainties of certain parameters, this discrepancy may still seem very high. Note, however, that we significantly overestimate the relevant chlorate content as only the immediate vicinity of the surface was probed. On the basis of electrostatic attractions, this is the region where most chlorate ions are expected to be found. Significant ion migration in a solid film has been described in ref 47. On the basis of the excessive amount of chlorate ions found at the PCBM surface, we can justify that electrostatic forces should play a major role. A more detailed analysis of the consequences of this model will be presented in a follow-up paper.

Conclusions

AFM snapshots revealed the rich variety of morphologies obtained by spin coating blends of PCBM and two cationic dyes from solution. We demonstrated that films form a transient bilayer which finally is destabilized through effective interface interactions. The stability of a system with bound counterions is well described by the stability conditions as predicted from van der Waals-type film destabilization. This makes us believe that convective flows during spin coating do not play a major role during the structure formation. For the system with mobile counterions we favor a model that describes a film destabilization mechanism of electrostatic origin. The following observations support this preference: (i) The PCBM−CyC system is always unstable as is the model with mobile counterions. (ii) A system without a mobile counterion exhibits no instabilities as predicted by this model. (iii) Electrostatic pressures exceed the van der Waals pressures for film thicknesses larger than ∼50−100 nm. (iv) The electrostatic free energy leads to a dominant wavelength that scales with the film thickness with an exponent of 1.5 as can be found by optimizing the time constant with respect to the wavelength for thin films.[11] The reasoning is analogous to that of ref 11, where instead of the van der Waals pressure ($\sim 1/h^3$) the electrostatic pressure ($\sim 1/h^2$) is used. The value 1.5 is closer to the experimental value 1.18 than for pure van der Waals forces, where this scaling exponent is 2. (v) The free energy contribution contains the dielectric constant and has a form analytically different from that of the van der Waals expression and may be able to explain certain features that seem to be specific for the free counterion system.

One merit of the material system is the monodispersity of the domains. In addition, the domain size depends on the film thickness, which can be varied easily. Thus, we guess that even smaller domains than the observed ∼30 nm features can be produced. The quest for smaller domains should not be considered as an end in itself; indeed, phase-separated domains with dimensions in the exciton diffusion range, which means ≤20 nm, are, for example, highly desired for the fabrication of organic photovoltaic cells. PCBM is one of the best known electron acceptors in heterojunction organic solar cells, and PCBM domains strongly suggested to originate from a similar liquid−liquid dewetting mechanism have been observed during phase separation of polythiophenes and PCBM.[54] In addition, already a strict bilayer of CyC and C_{60} has been demonstrated to function well as a photovoltaic device.[55] An understanding of the underlying domain formation processes is of crucial importance for the performance increase of such organic thin-film devices.

Acknowledgment. We thank M. Nagel for helpful discussion. We are grateful to T. Kuenniger for the dynamic contact angle measurements and U. Müller for the XPS measurements. We appreciate the disposal of the Swiss Scanning Probe Microscopy User Laboratory at Empa and P. Kappenberger for his support. We acknowledge funding from COST.

LA800099J

(51) Groenewold, J.; Kegel, W. K. *J. Phys. Chem. B* **2001**, *105*, 11702–11709.
(52) Groenewold, J.; Kegel, W. K. *J. Phys.: Condens. Matter* **2004**, *16*, S4877−S4886.
(53) Muratov, C. B. *Phys. Rev. E* **2002**, *66*, 66108.
(54) Nguyen, L. H.; Hoppe, H.; Erb, T.; Günes, S.; Gobsch, G.; Sariciftci, N. S. *Adv. Funct. Mater.* **2007**, *17*, 1071–1078.
(55) Fan, B.; Hany, R.; Moser, J.-E.; Nüesch, F. *Org. Electron.* **2008**, *9*, 85–94.